

Foundation Model–Driven Semantic Change Detection in Remote Sensing Imagery

Hengtong Shen, Li Yan, Hong Xie, Yaxuan Wei, Xinhao Li, Wenfei Shen, Peixian Lv and Fei Tan

Abstract—Remote sensing (RS) change detection methods can extract critical information on surface dynamics and are an essential means for humans to understand changes in the earth’s surface and environment. Among these methods, semantic change detection (SCD) can more effectively interpret the multi-class information contained in bi-temporal RS imagery, providing semantic-level predictions that support dynamic change monitoring. However, due to the limited semantic understanding capability of the model and the inherent complexity of the SCD tasks, existing SCD methods face significant challenges in both performance and paradigm complexity. In this paper, we propose PerASCD, a SCD method driven by RS foundation model PerA, designed to enhance the multi-scale semantic understanding and overall performance. We introduce a modular Cascaded Gated Decoder (CG-Decoder) that simplifies complex SCD decoding pipelines while promoting effective multi-level feature interaction and fusion. In addition, we propose a Soft Semantic Consistency Loss (SSCLoss) to mitigate the numerical instability commonly encountered during SCD training. We further explore the applicability of multiple existing RS foundation models on the SCD task when equipped with the proposed decoder. Experimental results demonstrate that our decoder not only effectively simplifies the paradigm of SCD, but also achieves seamless adaptation across various vision encoders. Our method achieves state-of-the-art (SOTA) performance on two public benchmark datasets, validating its effectiveness. The code is available at <https://github.com/SathShen/PerASCD.git>.

Index Terms—Foundation model, semantic change detection, modular decoder, remote sensing, deep learning.

I. INTRODUCTION

SEMANTIC change detection (SCD) or multi-class change detection have emerged in recent years as a RS interpretation task that has been receiving increasing attention. Unlike conventional binary change detection (BCD), SCD does not merely identify *where* changes have occurred, it

Manuscript received xx xx, 2026; revised xx xx, 2026; accepted xx xx 2026. Date of publication xx xx 2026; date of current version xx xx 2026. This work was partially supported by the Zhejiang Province "Vanguard" and "Geese Leading" Research and Development Plan under Grant 2025C01073, the National Natural Science Foundation of China under Grant 42394061, and the Natural Science Foundation of Wuhan under Grant 2024040701010028. (Hengtong Shen and Li Yan are co-first authors.) (Corresponding author: Hong Xie.)

The authors are with the School of Geodesy and Geomatics, Wuhan University, Wuhan 430079, China (e-mail: shenht@whu.edu.cn; lyan@sgg.whu.edu.cn; hxie@sgg.whu.edu.cn; weiyaxuan@whu.edu.cn; lkh17866703382@163.com; 15505084554@163.com; lvpeixian@whu.edu.cn; 2024282140087@whu.edu.cn).

Digital Object Identifier xxxxxxxxxxxxxxxxxxxxxxxxx

further specifies the *from-to* semantics of those changes (i.e., the class transition). This capability enables the extraction of semantic-level change maps from RS imagery, supporting more accurate urban planning [1], natural resource management [2], and disaster assessment [3].

Binary change detection (BCD) extracts change information and focus on detecting the locations of changed pixels. Due to the disregard for pixels' categories, BCD often fails to characterize the semantic change information required in downstream applications. Semantic change detection (SCD) networks can not only predict the precise locations of change areas but also provide detailed land-cover class information across multiple temporal images. However, the challenges of multi-class annotation, the complexity of semantic change tasks, and the relatively low demand for semantic change tasks, most existing change detection studies have focused on BCD. With advances in deep learning and RS imaging technologies, researchers are no longer satisfied with merely locating changes. Instead, there is a growing need to identify the specific types of change to support more precise decision-making across diverse domains.

In recent years, numerous SCD algorithms based on deep neural networks have been proposed, which have achieved impressive progress and played an important role in multiple fields. However, current SCD algorithms still suffer from various deficiencies ranging from model design to task logic, which significantly impair the network's performance in SCD tasks. In general, these limitations can be summarized into the following three points: (1) Existing methods invariably employ lightweight encoders which pre-trained with natural images, thereby failing to furnish accurate representations of RS features or precise semantic comprehension. (2) Existing methods are still constrained by category imbalance of SCD task, wherein the predominance of unchanged regions significantly exacerbates training difficulties, predisposing models to rely on simplistic shortcut solutions. (3) The decoders designed by existing methods are predominantly three-path explicit decoding structures, suffer from insufficient feature interaction, or exhibit overly complex architectures.

Existing SCD methods lack advanced semantic encoding capabilities, and recent progress in RS foundation models has provided a promising direction for addressing this issue. Foundation models are large-scale deep learning models that undergo massive pre-training on vast and diverse datasets, possess powerful general capabilities, and can be adapted to multiple downstream tasks through techniques such as fine-tuning. In recent years, various remote sensing foundation models pre-trained on RS imagery have been progressively

proposed [4], [5], [6], demonstrating outstanding performance across multiple remote sensing downstream tasks. However, although RS foundation models can provide strong semantic understanding capabilities for a wide range of downstream tasks, there has been remarkably little exploration by researchers in the field of SCD.

Starting from these issues to be resolved, we propose leveraging self-supervised pre-trained foundation models to endow SCD with robust semantic encoding capabilities. We aim to leverage a well-pre-trained semantic extractor to derive change features from the abundance of invariant features. Specifically, we leverage PerA [7], a foundation model pre-trained leveraging self-supervised learning, to achieve more precise semantic understanding. To achieve better adaptation to RS foundation models, enhance information interaction among features within the model, and simplify the SCD paradigm, we propose a modular decoder called Cascaded Gated Decoder (CG-Decoder). The decoder learns and controls the feature weights at different scales through a Change-Aware Gating Module (CAGM), simultaneously accomplishing feature dimensionality reduction, feature fusion, and feature upsampling. This design effectively alleviates the class imbalance problem commonly encountered in SCD tasks. Furthermore, we investigated the performance of different RS foundation models and encoders on the SCD task, and discussed the potential numerical instability issues that may arise in the commonly used SCLoss for SCD. Our contributions can be summarized as follows:

- (1) We propose the Cascaded Gated Decoder (CG-Decoder), a modular decoder that seamlessly achieves feature compression, multi-level fusion, upsampling, and precise change extraction. The decoder enables effective adaptation between multi-scale features and heterogeneous outputs, simplifying the paradigm of SCD. Empowered by large-scale RS foundation PerA, our framework achieves state-of-the-art (SOTA) performance on multiple SCD benchmarks, and extensive comparisons with existing methods demonstrate its superior effectiveness.
- (2) The first comprehensive investigation into the applicability of RS foundation models for SCD is conducted. We systematically evaluate representative RS foundation models and encoders across different paradigms. Our results reveal that, combined with our proposed decoder, these models can effectively handle SCD tasks. This not only validates their feasibility but also fills a significant research gap in this underexplored area.
- (3) A comprehensive analysis of the potential numerical instability issues inherent in SCLoss is conducted, and a novel Soft Semantic Consistency Loss (SSCLoss) is proposed to enhance the training stability of SCD models. Experimental results demonstrate that our proposed loss effectively mitigates numerical instability problems triggered under specific conditions during training, providing a valuable reference for the training of large-scale SCD models.

II. RELATED WORK

In this section, we review the current state of RS foundation models and the development of BCD and SCD methods. We particularly focus on the evolution of SCD architectural paradigms.

A. RS Foundation Model

Foundation models are general-purpose models pre-trained on large-scale, diverse datasets. RS foundation models, pre-trained on vast RS data and tailored to its unique characteristics, outperform general models pre-trained on natural images in RS interpretation tasks, demonstrating superior generalization and domain-specific capabilities. Recent advances in self-supervised learning have produced numerous RS foundation models to address high annotation costs. Generative approaches include RingMo [5] and Scale-MAE [8], while contrastive learning-based methods such as SeCo [9] and SkySense [10] have gained prominence due to their effectiveness and flexibility. These studies demonstrate the strong potential of self-supervised pre-training for RS tasks. SCD demands strong semantic understanding to accurately capture "from-to" transitions, making RS foundation models a highly promising direction for advancing SCD.

B. Binary Change Detection

Early change detection methods were predominantly focused on binary change detection (BCD). Traditional BCD approaches relied heavily on handcrafted features and pixel-wise classifiers to generate binary change maps, suffering from limited accuracy and poor generalization capability. With the advent of deep Convolutional Neural Networks (CNNs) and Transformers, deep learning-based methods have gradually replaced conventional techniques, achieving substantial performance improvements in BCD tasks. Most deep learning-based methods for BCD employ siamese-like network architectures to extract features from bi-temporal images, followed by difference comparison and feature fusion to predict binary change regions. In the early stages, methods such as FC-Siam-conc [11] and SNUNet-CD [12] utilized purely CNN structures for BCD tasks. Following the widespread adoption of ViTs [13], ViT-based or CNN-ViT hybrid approaches like BIT [14], ChangeFormer [15], have gained prominence. In recent works on RS foundation models [5], [10], has been commonly employed as a key downstream task for model evaluation. However, in the contrast, SCD has received scarcely any attention in this context.

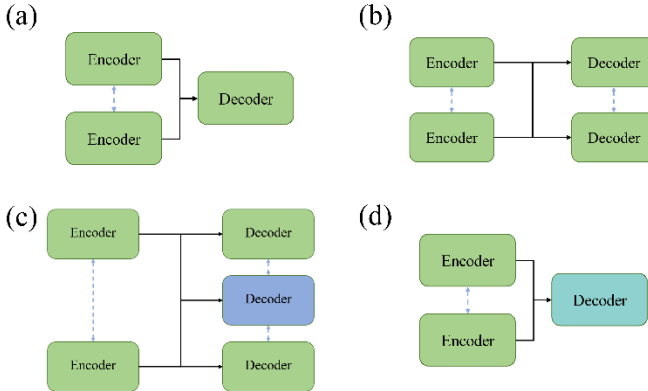


Fig. 1. Existing common paradigms of semantic change detection models.

C. Semantic Change Detection

Early explorations in pixel-level SCD were predominantly either non-end-to-end approaches [16] or methods that only output post-change semantic classifications [17], [18]. These approaches exhibit certain limitations in terms of prediction accuracy and usability. HRSCD [19] is widely regarded as the pioneering effort that aligns with the contemporary definition of SCD, establishing the foundation for "from-to" change outputs. It systematically investigated the feasibility of various network architectures in this context. Subsequently, multiple end-to-end SCD methods have been continually proposed. As shown in Fig. 1, most SCD methods employ siamese-like dual-temporal encoders like BCD methods and can be straightforwardly categorized into single-branch, dual-branch, triple-branch and fused decoding approaches. The blue dashed lines indicate potential feature interactions, while the blue decoder is specifically designed to process the fused change features. Among these, single-branch methods such as HRSCD str2, treat each possible "from-to" change combination as an independent class for prediction. While this strategy is conceptually straightforward, it suffers from performance limitations due to the quadratic growth in the number of required classification categories. Dual-branch methods like DCCANet [20] and SCDNet [21], closely approximate the ideal paradigm of SCD by bi-temporal feature extraction and independent semantic classification, and then generate change masks from classification maps. However, multiple studies have demonstrated that these methods exhibit inferior performance compared to three-branch methods. Consequently, they are gradually being supplanted by the latter. In recent years, triple-branch methods have gained widespread popularity. The majority of these approaches involve a separate, explicit decoder specifically designed to process change information. Representative works, such as SemanticCD [22], MCDnet [23], GCF-SCD-Net [24], and SCanNet [25], all adopt this architectural paradigm, albeit with differing strategies for inter-branch feature fusion. However, the drawbacks of this paradigm are evident: since change regions can be directly derived through the simple binarization of classification maps, processing change masks separately inevitably leads to increased network complexity

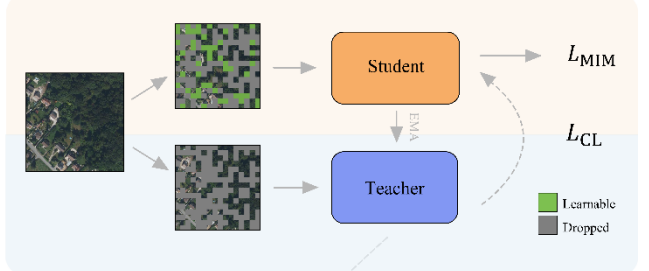
and is often considered superfluous. Fig. 1(d) illustrates the SCD paradigm used in this work. The cyan decoder represents the module that fuses the separated pre-change semantic features, post-change semantic features, and the change feature decoder, enhancing the interaction among decoded features while reducing the complexity of the model paradigm.

Furthermore, beyond innovations in architectural paradigm design, novel breakthroughs in other aspects of SCD have also contributed substantially to the improvement of model performance. Since the change class is severely underrepresented, its contribution to the expected gradient is often negligible within a mini-batch, causing the overall gradient expectation to be biased toward the non-change class. Bi-SRNet [26] proposed SCloss to align the semantic and change representations alleviating the problem to some extent. However, the loss function may introduce training numerical instability under certain conditions. We propose SSCLoss in this work to mitigate this issue, which is described in detail in Section III-D. Auxiliary information from other modalities has also been explored to enhance performance. For instance, MSCD-Net [27] incorporates SAR imagery and DSM data to aid semantic understanding, demonstrating significant advantages. RB-SCD [28] incorporates text and frequency domain information into the network, providing a new approach to SCD methods. Furthermore, several recent works like Mamba-FCS [29] and GSTM-SCD [30] employ new encoder architectures to improve efficiency and performance, providing new insights for SCD model designing.

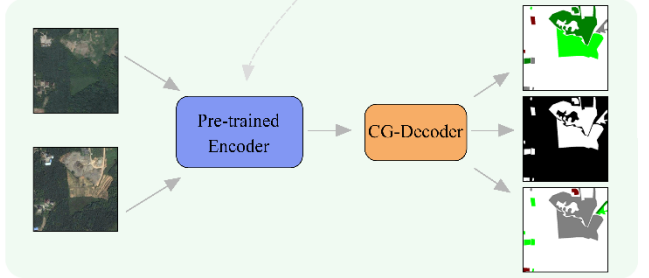
III. METHOD

In this section, we first briefly introduce the pre-trained model and fine-tuning strategy adopted in this work. We then present the overall framework of PerASCD. Subsequently, the Cascaded Gated Decoder and Change-Aware Gating Module are described in detail. Finally, we introduce the Soft Semantic Consistency Loss.

(a) PerA Pre-training



(b) PerASCD Fine-tuning



> REPLACE THIS LINE WITH YOUR MANUSCRIPT ID NUMBER (DOUBLE-CLICK HERE TO EDIT) <

Fig. 2. Overall pipeline: (a) Illustration of PerA pre-training; (b) Illustration of PerASCD fine-tuning.

A. Overall pipeline

As shown in the Fig. 2(a), the PerA pre-training method is a self-supervised learning approach that integrates the strengths of contrastive learning and mask image modeling. Specifically, the PerA replaces random cropping in the regular pretext task of contrastive learning with random masking and incorporates learnable mask tokens into the input patches. This design enables the model to acquire global semantic understanding from RS images via contrastive objectives while simultaneously capturing fine-grained local semantic details through pixel-level reconstruction, significantly enhancing the inherent capability of the ViT model for semantic feature extraction and comprehension in RS imagery. After pre-training, we employ the encoder from the teacher, a standard ViT as the pre-trained backbone for downstream transfer learning.

As illustrated in Fig. 2(b), after the pre-training stage, the pretrained encoder is adopted as the backbone of PerASCD and combined with the CG-Decoder for fine-tuning on the SCD task. We employ ViT-Adapter [31] to enhance the pretrained model with stronger spatial priors, improving pixel-level prediction accuracy and enabling the extraction of multi-scale features. The multi-scale features generated by the encoder are progressively processed, upsampled, and fused by

the CG-Decoder, ultimately producing both the bi-temporal semantic change map and the binary change map. Detailed descriptions of PerASCD and the adopted CG-Decoder are provided in the subsequent sections.

B. Architecture of PerASCD

The overview of proposed PerASCD architecture is shown in Fig. 3. PerASCD adopts a simple encoder-decoder architecture and leverages the PerA method which is self-supervised pre-trained via contrastive learning on massive unlabeled RS image tiles. PerASCD first extracts multi-scale, semantically feature maps using the PerA pre-trained ViT encoder and ViT-Adapter. Given the bi-temporal RS images $X_A, X_B \in R^{C \times H \times W}$, the pre-trained model processes them into multi-scale feature maps $F_{A,1}, F_{B,1}, \dots, F_{A,4}, F_{B,4}$. These features are then progressively processed through CG-Decoder blocks. This cascaded multi-scale feature processing paradigm draws inspiration from U-Net's skip connections [32]. We will provide a detailed description of this in Subsection C. Through this design, the CG-Decoder achieves efficient feature compression, multi-level semantic fusion, precise change extraction, and multi-scale upsampling within a simple, modular framework. Finally, the features are processed and fused into a unified set of features, which are then fed into the classifier to produce the final binary change map and the semantic maps.

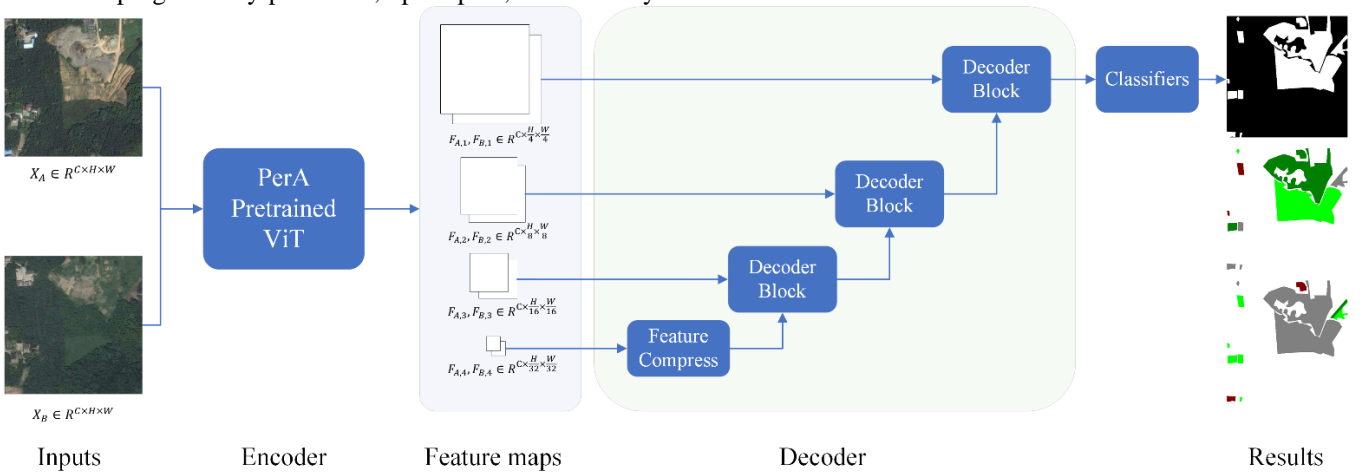


Fig. 2. Architecture of PerASCD.

C. Cascaded Gated Decoder and Change-Aware Gating Module

The Cascade-Gated Decoder (CG-Decoder) represents the core innovation in PerASCD, enabling effective semantic change decoding of multi-scale bi-temporal features. Through high-dimensional feature compression, multi-level feature fusion, feature upsampling, and change-aware gating, it transforms complex multi-scale features into large-scale pixel-level semantic representations suitable for classification. This decoder simultaneously addresses feature dimensionality reduction, fusion, and upsampling while accommodating diverse encoder input requirements, simplifying and streamlining the SCD task. The structure of a single CG-

Decoder Block is illustrated in Fig. 4(a).

The Cascade-Gated Decoder is composed of multiple CG-Decoder Blocks, facilitating modular multi-scale feature fusion and change information extraction. Specifically, the CG-Decoder block n first processes smaller-scale deep features from previous block $x_{A,n}$, $x_{B,n}$, and $x_{C,n}$ representing pre-change, post-change, and change features, respectively. The two temporal features are passed through a dual-layer convolutional network for processing. Subsequently, the three features are concatenated to integrate semantic and change information, and then fed into another dual-layer convolution to yield a more refined change representation. Following this, the three features undergo upsampling to align with the shallow features' resolution. This process can be formulated

> REPLACE THIS LINE WITH YOUR MANUSCRIPT ID NUMBER (DOUBLE-CLICK HERE TO EDIT) <

as:

$$h_A, h_B = \text{DoubleConv}(x_{A,n-1}, x_{B,n-1}) \quad (1)$$

$$h_C = \text{DoubleConv}(\text{Cat}(x_{C,n-1}, h_A, h_B)) \quad (2)$$

$$h'_A, h'_B, h'_C = \text{Upsample}(h_A, h_B, h_C) \quad (3)$$

where h'_A , h'_B , and h'_C are the upsampled features, and Cat denotes the vector concatenation operation. Larger-scale shallow features are directly sourced from the encoder outputs. Their processing mirrors that of deep features, but replaces the dual-layer convolution with a feature compress layer and the concatenation with pixel-wise differences between the pre- and post-change features. The initial deep features $x_{A,N}$, $x_{B,N}$, and $x_{C,N}$ in first block are processed similarly. This can be expressed as:

$$z_{A,n-1}, z_{B,n-1} = \text{FC}(F_{A,n-1}, F_{B,n-1}) \quad (4)$$

$$z_{C,n-1} = \text{FC}(\text{abs}(z_{A,n-1} - z_{B,n-1})) \quad (5)$$

where $z_{A,n-1}$, $z_{B,n-1}$, and $z_{C,n-1}$ are the compressed features, FC denotes the feature compression layer, and abs represents the absolute value operation. The FC layer employs the CBAM alongside a single-layer convolution for feature compression, minimizing information loss under minimal computational overhead. When high-dimensional features f are input into FC layer, the process be expressed as:

$$f' = \text{CBAM}(f) \quad (6)$$

$$f'' = \text{ConvCompress}(f') \quad (7)$$

where ConvCompress is a convolutional layer that maps the input features to the desired output dimension. The f' denotes the features processed through the CBAM attention mechanism to minimize information loss, while f'' represents

(a) Cascaded Gated Decoder

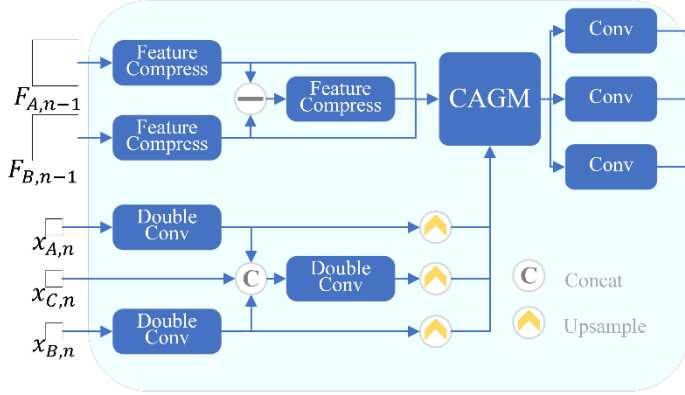


Fig. 4. (a) Architecture of Cascaded Gated Decoder; (b) Architecture of Change-Aware Gating Module.

D. Soft Semantic Consistency Loss

The Semantic Consistency Loss (SCLoss) is designed to align the semantic and change representations, and has been experimentally validated to substantially mitigate the class imbalance problem, enhancing the overall performance of SCD models. Given two feature vectors x_1 and x_2 , the formula for SCLoss can be expressed as:

$$L_{SC} = \begin{cases} 1 - \cos(x_1, x_2), & \text{if } y = 1 \\ \max(0, \cos(x_1, x_2) - m), & \text{if } y = -1 \end{cases} \quad (12)$$

the compressed features.

The processed shallow and deep features are both fed into the Change-Aware Gating Module (CAGM) for fusion, and subsequently passed through a convolutional layer for additional fusion processing, yielding $x_{A,n-1}$, $x_{B,n-1}$, and $x_{C,n-1}$, which serve as inputs to the next CG-Decoder block. The structure of the Change-Aware Gating Module is illustrated in Fig. 4(b). The CAGM first concatenates the input change features and generates global and local weighted feature representations with convolution layers. These representations are then transformed into probabilities W_{global} and W_{local} via Sigmoid function. We calculate final weights as $(1 + W_{global})W_{local}$, which are then assigned to each feature input to the module. Subsequently, the weighted features are added together in a pixel-wise, and output to the final fusion convolution. This process can be succinctly summarized by the following formulation:

$$W_{local} = \sigma(\text{Conv}(\text{Cat}(h'_C, z'_C))) \quad (8)$$

$$W_{global} = \sigma(\text{Conv}(\text{GAP}(\text{Cat}(h'_C, z'_C)))) \quad (9)$$

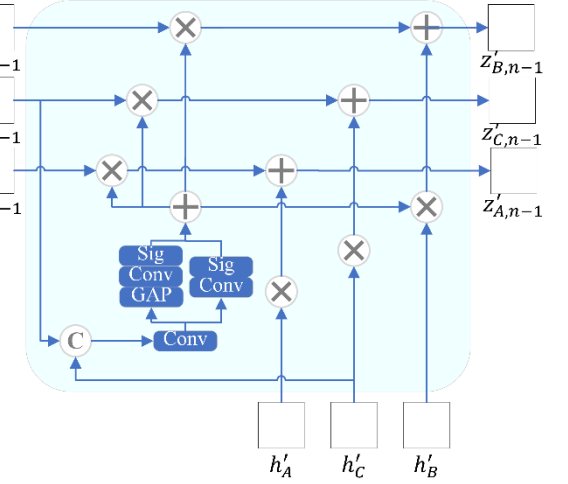
$$[W_z, W_h] = (1 + W_{global})W_{local} \quad (10)$$

$$z'_{i,n-1} = \text{Conv}(W_z * z_{i,n-1} + W_h * h'_i) \quad (11)$$

where $i \in \{A, B, C\}$, σ denotes Sigmoid function, and GAP denotes global average pooling.

Finally, after passing through multiple CG-Decoder blocks, the bi-temporal semantic features and the change features are respectively fed into the classifier to compute probabilities, yielding the prediction results.

(b) CAGM



where \cos denotes the cosine similarity and m denotes a constant margin which is usually set to 0.1. The y denotes the binary change label, with $y = 1$ indicating no change and $y = -1$ indicating a change.

However, we observe that the optimization process may exhibit training instability under certain conditions. While other factors, such as learning rate and mixed-precision training, may also contribute, the instability is observed to be substantially mitigated upon disabling the original SCLOSS.

> REPLACE THIS LINE WITH YOUR MANUSCRIPT ID NUMBER (DOUBLE-CLICK HERE TO EDIT) <

Therefore, we hypothesize that these issues are due to a limitation in the mathematical formulation of SC Loss. Specifically, owing to the introduction of the margin in the SC Loss, when the feature distribution undergoes drastic changes, the cosine similarity values near the margin boundary may abruptly cross the threshold. Consequently, the gradient with respect to the feature representations can suddenly vanish or switch from zero to a non-zero value, leading to severe loss fluctuations or unstable gradient behavior during training. This issue becomes more pronounced when a large learning rate is

adopted, especially in conjunction with mixed-precision training.

As illustrated in Fig. 5, such issue manifests as cliff-like dips in the accuracy curves during the training process. Furthermore, through monitoring, we can clearly observe that a large proportion of pixel-wise cosine similarities exceed the margin sharply when instability events occur. Accordingly, the F_{scd} values on validation set exhibit a sudden degradation corresponding to pronounced fluctuations in the loss curve.

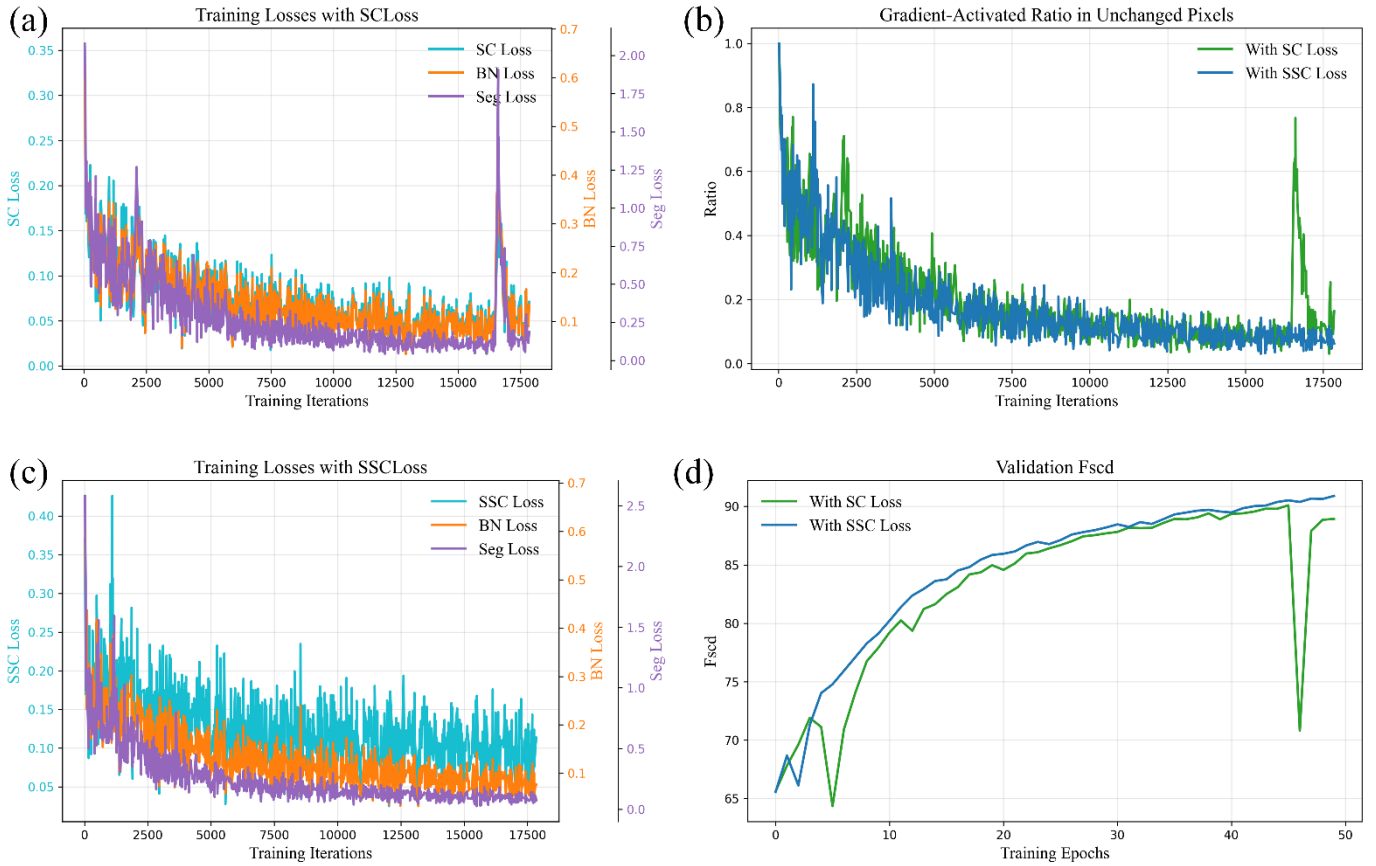


Fig. 5. Training curves under numerical instability (a) Training losses with SC Loss; (b) Gradient-activated ratio in unchanged pixels with different loss; (c) Training losses with SSC Loss; (d) Validation F_{scd} with different loss.

To this end, we design a novel loss function called Soft Semantic Consistency Loss (SSCLoss) to mitigate the numerical instability while preserving the original representation alignment capability. The formulation of SSCLoss can be expressed as:

$$L_{SSC} = \begin{cases} 1 - \cos(x_1, x_2), & \text{if } y = 1 \\ \tau \text{Softplus}\left(\frac{\cos(x_1, x_2) - m}{\tau}\right), & \text{if } y = -1 \end{cases} \quad (13)$$

where:

$$\text{Softplus} = \log(1 + \exp(x)). \quad (14)$$

The Softplus replace the hard hinge margin with a smooth approximation, leading to continuous gradient transitions. The temperature parameter τ jointly controls the width of the transition region around the margin and the amount of gradient leakage inside the margin, by rescaling both the argument and the magnitude of the softplus function. We empirically adjust τ for different dataset to ensure a smooth transition of gradient

activation around the margin while preserving the discriminative role of the margin. This design preserves the acceptable region for feature similarity constraints defined in the original loss function, while preventing large-scale gradient population migration, significantly mitigating the likelihood of numerical instability. We will discuss this in detail in the ablation experiments of Chapter IV.

IV. EXPERIMENTS

A. Datasets

We evaluate our method on the SEmantic Change detectiON Dataset (SECOND) [33] and LandsatSCD [34], which are publicly available benchmark datasets for SCD.

The SECOND is consist of 4662 pairs of aerial images in a high-resolution from several platforms and sensors. These pairs of images are distributed over the cities, such as

> REPLACE THIS LINE WITH YOUR MANUSCRIPT ID NUMBER (DOUBLE-CLICK HERE TO EDIT) <

Hangzhou, Chengdu, and Shanghai. Each image has been cropped into 512×512 size and is annotated at the pixel level. The images are in a spatial resolution varies from 0.5 to 3 m/pixel. Each semantic change label has been annotated by a professional labeling group and classified into seven categories: non-change, non-vegetated ground surface, tree, low vegetation, water, buildings, and playgrounds. We adopt the standard split of 2,968 training pairs and 1,694 test pairs for our experiments following previous work.

The LandsatSCD is collected between the years 1990 and 2020 in Xinjiang, China. The dataset contains 8,468 pairs of bi-temporal image patches, most of which are generated through data augmentation. After filtering, a total of 2,385 image pairs are retained. Following previous work, we split the dataset into training, validation, and test sets with a ratio of 3:1:1, resulting in 1,431, 477, and 477 image pairs, respectively. Collected from Landsat satellite, the images in dataset are all in a resolution of 30m/pixel. All of them are annotated for changes across four land cover classes—farmland, desert, buildings, and water bodies.

B. Implementation Details

All experiments are implemented using PyTorch and conducted on NVIDIA GeForce 4090. To ensure reproducibility, a fixed random seed is applied to all experiments. The proposed method is trained using stochastic gradient descent (SGD) optimizer with momentum. We adopt a ViT-G/16-1024 model pre-trained by PerA with ViT-Adapter as the backbone. The batch size is set to 8 and the weight decay is set to 1e-5. To improve training stability and efficiency, mixed-precision training is employed using automatic mixed precision (AMP) with gradient scaling. For SECOND dataset, the initial learning rate is set to 0.1 with a momentum of 0.9, and decays to zero following a polynomial schedule. A linear warm-up phase occupying the first 10% of total training iterations to enhance stability. For LandsatSCD dataset, due to its relatively simpler data distribution, we set the initial learning rate to 1.0 with a minimum learning rate of 0.5. Except for replacing SCLoss with our proposed SSCLoss, we utilize exactly the same loss functions as SCanNet to train our model.

C. Comparison with other SCD methods

We compare our proposed method with other SCD methods on standard benchmark datasets, including former state-of-the-

art to demonstrate the effectiveness and generalization ability of our approach. These methods including: 1) classic SCD method HRSCD [19] which proposed basic paradigms; 2) SSCDI [26] and BiSRNet [26] which proposed SCLoss; 3) TED [25] and SCanNet [25] which integrated transformer; and 4) Mamba-FCS [29] which is recently published SCD method that utilizes the Mamba architecture. For fair comparison, all methods adopted experimental setup in the original paper and are evaluated under the same preprocessing and training settings whenever possible. Following previous works, we report best Overall Accuracy (OA), SCD-targeted F_1 score (F_{scd}), mean Intersection over Union (mIoU), and Separated kappa (Sek) on the test sets. All experiments are conducted using the same training/test split and input resolution.

As shown in the Table I, our method outperforms the compared approaches across all metrics. Particularly, the F_{scd} is improved by 2.88% over the baseline SCanNet on the challenging dataset SECOND, and 4.01% on the LandsatSCD dataset. Compared to the previous state-of-the-art Mamba-FCS, our method improves the F_{scd} by 0.63% on the SECOND dataset and by 1.63% on the LandsatSCD dataset. The performance gains can be attributed to the strong semantic representations provided by PerA, the incorporation of prior knowledge through CAGM, and the more stable training enabled by SSCLoss.

Fig. 6 (a) and Fig. 6 (b) illustrate qualitative comparisons on SECOND dataset and LandsatSCD dataset respectively. To better highlight the superiority of our method, we selected test examples from the two datasets that exhibit diverse land cover types, complex objects, and demand fine-grained predictions. Our approach produces more precise boundaries and reduces false positives in complex change regions compared to all other methods. In scenarios that require fine-grained prediction, our model generally outperforms all other methods, clearly separating multiple buildings or delineating the contours of changing rivers. In the third example from the SECOND dataset, our model is the only one that successfully identifies the otherwise inconspicuous tennis court next to the playground, demonstrating the advantages of semantic understanding provided by RS foundation model.

The comparative experiments demonstrate the superior performance of our proposed method, showing clear quantitative improvements on both simple and complex datasets, which validates the effectiveness of our approach.

> REPLACE THIS LINE WITH YOUR MANUSCRIPT ID NUMBER (DOUBLE-CLICK HERE TO EDIT) <

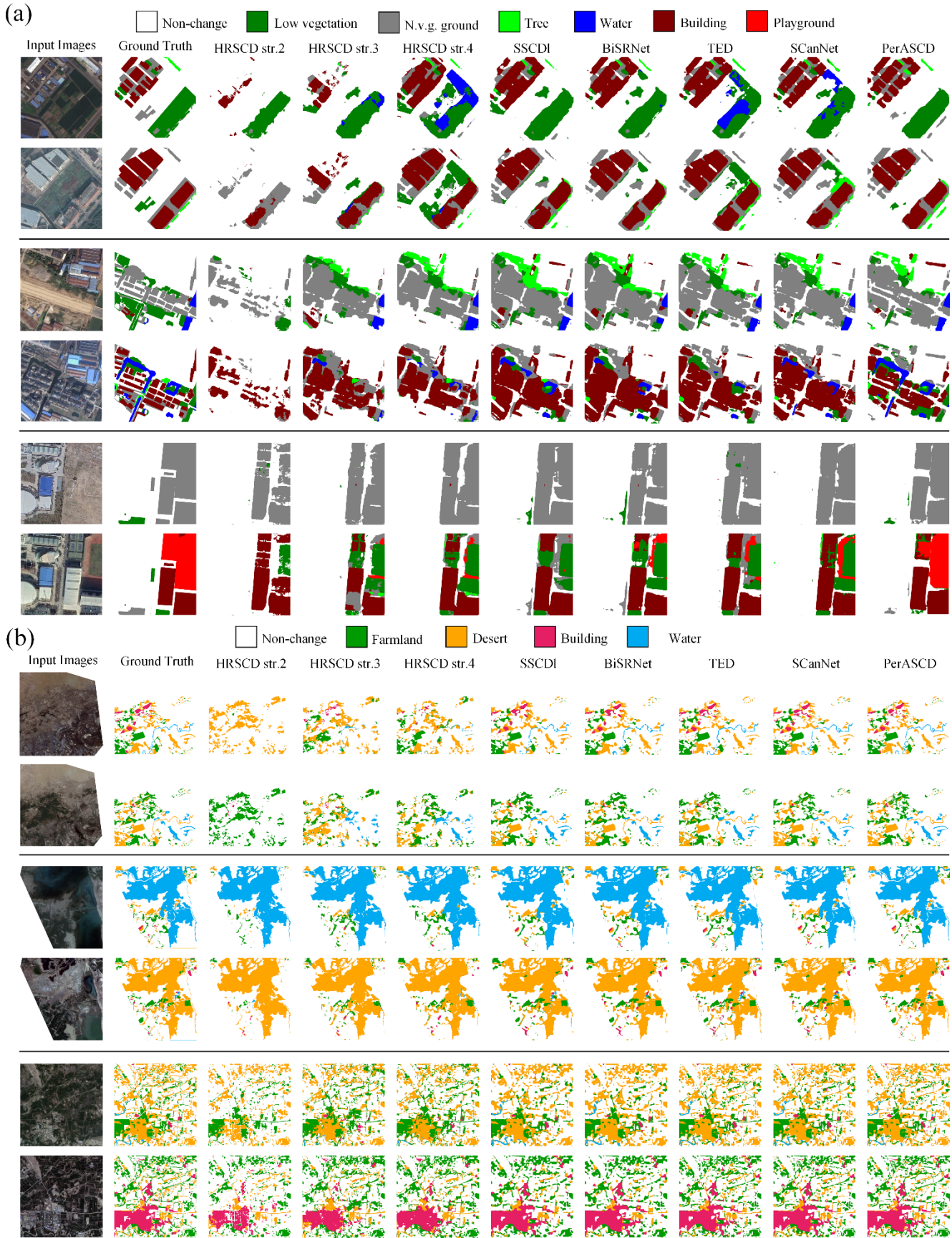


Fig. 6. Examples of results provided by different methods in the comparative experiments. (a) Results on the SECONd dataset; (b) Results on the LandsatSCD dataset.

> REPLACE THIS LINE WITH YOUR MANUSCRIPT ID NUMBER (DOUBLE-CLICK HERE TO EDIT) <

TABLE I
COMPARISON WITH OTHER SCD METHODS, * INDICATES RESULTS REPRODUCED FROM PAPERS WITHOUT PUBLIC CODE AND
BOLD INDICATES THE BEST RESULT.

Method	SECOND				LandsatSCD			
	OA	F_{scd}	mIoU	Sek	OA	F_{scd}	mIoU	Sek
HRSCD Str. 2	85.69	51.24	65.05	11.60	90.67	70.71	73.55	25.09
HRSCD Str. 3	85.33	54.05	66.91	13.37	91.17	72.55	77.22	29.64
HRSCD Str. 4	87.25	60.22	71.97	20.13	91.96	74.77	79.32	33.39
SSCD1	87.25	62.72	73.02	22.75	94.32	83.59	84.31	47.60
BiSRNet	87.67	63.10	73.29	23.05	94.13	82.97	83.75	46.23
TED	87.49	62.94	73.06	22.67	95.43	86.62	87.12	54.69
SCanNet	87.57	63.53	73.03	23.18	95.42	86.89	86.96	54.77
Mamba-FCS*	88.62	65.78	74.07	25.50	96.25	89.27	88.81	60.26
PerASCD	88.70	66.41	74.33	26.11	96.84	90.90	90.54	65.21

D. Ablation studies

1) *Ablation Study with Different Backbone Encoders*: To investigate performance variations across different RS foundation models and vision encoders, and to evaluate the adaptability of the proposed CG-Decoder, we conduct an extensive ablation study by integrating it with various pre-trained backbones. These include ResNet [35], Swin Transformer [36], VMamba [37], , SatMAE [38], and SeCo [9]. As shown in Table II, the proposed framework demonstrates strong generalization across a wide range of backbone encoders, including CNNs, Mamba-based models, and Transformers, highlighting the architectural flexibility and robustness of the CG-Decoder. Among the evaluated backbones, both VMamba and Swin-L achieve competitive performance, indicating their strong representation capacity for semantic change detection. Notably, VMamba-B attains impressive results under a relatively limited parameter budget, demonstrating its high parameter efficiency. However, during training, we observe that VMamba-based models are more prone to numerical instability. This behavior can be attributed to the exponential nature of VMamba’s selective scan, which causes even slight weight perturbations to accumulate and explode over long sequences, resulting in numerical overflows and unstable optimization.

Regarding pre-training strategies, RS pre-training does not consistently outperform ImageNet pre-training across all settings. In particular, the SeCo pre-trained ResNet50 exhibits slightly inferior performance compared to its ImageNet pre-trained counterpart. This can be explained by two factors: first, SeCo is pre-trained on Sentinel-2 imagery, whose relatively lower spatial resolution may limit its suitability for high-resolution SCD; second, the relatively modest scale of the SeCo pre-training dataset may constrain the richness of the learned representations. In contrast, the model pre-trained with PerA achieves the best overall performance. Benefiting from large-scale RS pretraining dataset and a powerful foundation model architecture, PerA provides more transferable semantic representations that are well aligned with the requirements of SCD. These results suggest that large-scale RS foundation models are crucial for fully unlocking performance gains in

SCD.

TABLE II
ABLATION STUDY WITH DIFFERENT BACKBONE ENCODERS,
BOLD INDICATES THE BEST RESULT.

Encoder/Method	SECOND			
	OA	F_{scd}	mIoU	Sek
SCanNet	87.57	63.53	73.03	23.18
ResNet50	88.03	64.06	73.53	23.80
VMamba-B	88.02	65.31	73.87	25.10
Swin-L	88.19	65.74	73.91	25.40
ResNet50 (SeCo pre-trained)	87.62	63.00	72.86	22.67
ViT (SatMAE pre-trained)	88.12	64.92	73.65	24.62
ViT-G/16/1024 (PerA pre-trained)	88.70	66.41	74.33	26.11

2) *Ablation Study with Different Individual Improvements*: To investigate the contribution of each individual improvement in our method, we conduct an ablation study by selectively enabling or disabling each component. As shown in the Table III, we conducted ablation experiments on the pre-trained encoder, CG-Decoder, CAGM, and SSCLoss individually. All experiments were performed under the same settings, and the results are reported in terms of OA, F_{scd} , mIoU, and Sek on the SECOND dataset.

From the experimental results, we can observe that performance improvements are not limited to using the PerA pre-trained ViT. When combined with the CG-Decoder, a ResNet-50 backbone also achieves consistent gains across all metrics compared to the baseline SCanNet. Furthermore, the contribution of CAGM is highly pronounced: incorporating CAGM leads to a notable improvement of 0.79% in the F_{scd} . In addition, compared with the original SCloss, SSCLoss does not bring substantial performance enhancement. Instead, its primary benefit lies in enhancing the training stability and

> REPLACE THIS LINE WITH YOUR MANUSCRIPT ID NUMBER (DOUBLE-CLICK HERE TO EDIT) <

robustness of the model, as we discussed in Section III-D and further validated in item 3) of this section.

TABLE III
ABLATION STUDY WITH DIFFERENT INDIVIDUAL IMPROVEMENTS, BOLD INDICATES THE BEST RESULT.

Method	SECOND			
	OA	F_{scd}	mIoU	Sek
SCanNet	87.57	63.53	73.03	23.18
ResNet50+CG-Decoder	88.03	64.06	73.53	23.80
PerASCD (SCanNet Decoder)	88.35	65.95	74.14	25.72
PerASCD w/o CAGM	88.48	65.62	74.16	25.46
PerASCD w/ L_{sc}	88.87	66.39	74.36	26.07
PerASCD	88.70	66.41	74.33	26.11

To provide insights into the interpretability of CAGM, we visualize its learned gating weight maps. As shown in the Fig. 7, for each group of examples, the first and second rows present the original images, ground-truth, and model predictions, while the third and fourth rows illustrate the weight heatmaps of the deep features (low resolution) and shallow features (high resolution) learned by the CAGM in every CG-Decoder Block.

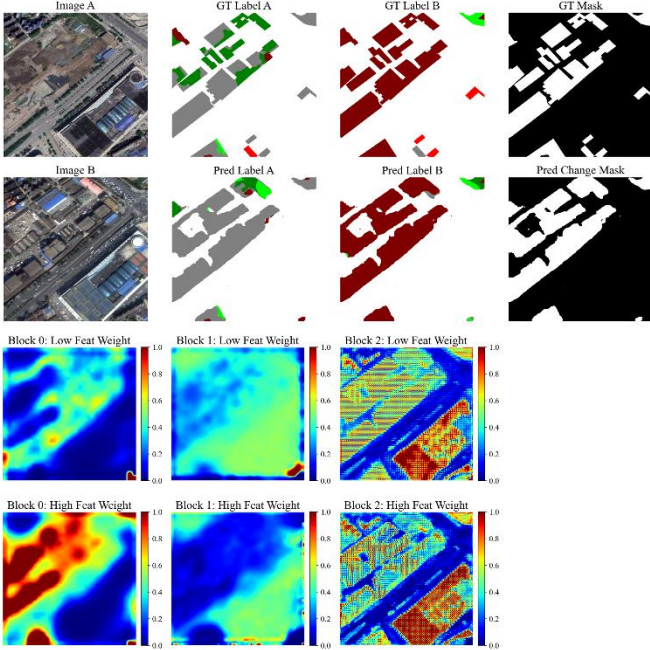
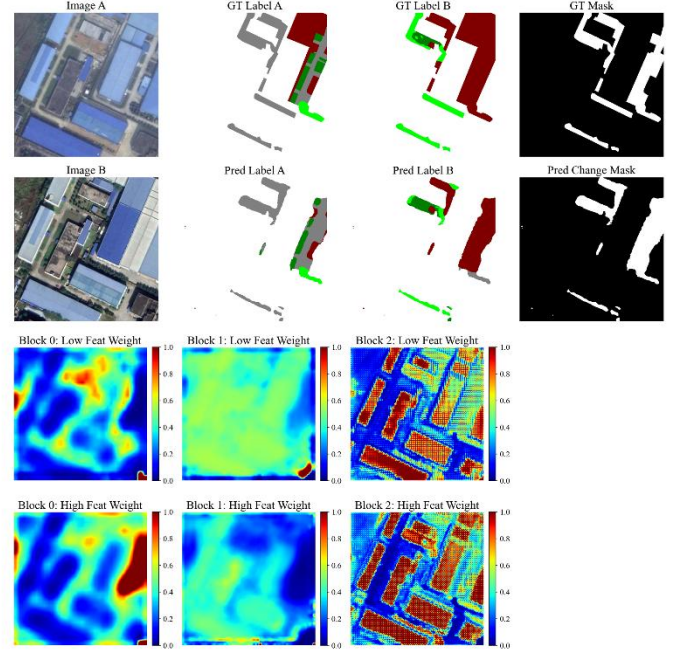


Fig. 7. Examples comparing CAGM weight heatmaps with the corresponding prediction results.

3) *Ablation Study of Numerical Instability on LandsatSCD Dataset:* We conduct detailed ablation experiments to explore the inner mechanism of the numerical instability and validate the effect of our proposed SSCLoss. Due to the relatively simple data distribution of LandsatSCD and the sufficient capacity and structural stability of the PerASCD, the network

From deep to shallow layers, we observe that the heatmaps align well with our design expectations. Although no explicit supervision is imposed to enforce the learning of correct change regions, the weight heatmaps predicted by the CAGM in each CG-Decoder Block generally delineate the boundary between changed and unchanged areas. As the feature maps are progressively upsampled in spatial resolution, the heatmaps become increasingly refined, with more accurate focus regions. We also experimented with using the ground-truth change masks as explicit learning targets; however, such rigid constraints instead limited the model’s performance.

From a semantic perspective, the learning process exhibits a clear progression from coarse to fine. In most cases, the model first roughly localizes the change regions using highly compressed deep semantic features, then learns the relatively simpler unchanged regions, and finally refines its attention to the change regions to capture fine-grained details. Notably, in the heatmaps of the final layers, the change regions are almost precisely outlined, yet they do not correspond to the highest-attention red regions. Instead, the change regions in heatmaps is concentrated in grid-like striped areas with moderate weight values, typically ranging from 0.3 to 0.7. We hypothesize that this phenomenon arises because the learned weights are jointly applied to both change features and semantic features; consequently, non-change objects that are prone to being misclassified as change regions require greater attention and thus receive higher emphasis.



is able to tolerate a relatively large learning rate. Empirically, we observe that PerASCD achieves its optimal performance on LandsatSCD with a learning rate as high as 1.0. However, we also observe that models incorporating the original SCloss may suffer from sporadic numerical instability. Moreover, the probability of such instability increases as the learning rate

> REPLACE THIS LINE WITH YOUR MANUSCRIPT ID NUMBER (DOUBLE-CLICK HERE TO EDIT) <

becomes larger due to the larger update step size. With an initial learning rate of 1.0 and a minimum of 0.5, the model achieves peak accuracy. However, numerical instability is nearly unavoidable, even under strict gradient clipping. In such cases, isolated unstable batches can trigger sudden, large drops in the loss and gradient values, manifesting as cliff-like deviations in the training curves. Additionally, we observe that using FP32 significantly reduces numerical instability. This is because while mixed-precision training lowers computational cost, it also increases the likelihood of gradient underflow, making small differences near the hinge margin more prone to being rounded to zero, which in turn sharply raises the probability of instability in the subsequent iterations.

During the early stages of training, we also observe fluctuations in the training curves that resemble numerical instability, but do not exhibit the characteristic cliff-like behavior. These fluctuations are not caused by gradient discontinuities near the margin, but rather stem from the randomness introduced by weight initialization. To ensure a fair and rigorous evaluation, we ignore such fluctuations occurring within the first five epochs. Numerical instability is defined as the occurrence of a cliff-like dip in performance during the subsequent training process. In multiple runs, the presence of numerical instability is determined if such an event occurs at least once.

As shown in the Table IV, we can clearly observe that the numerical instability issues are strongly correlated with floating-point precision and loss function. On the LandsatSCD dataset, when the maximum learning rate is set to 1.0 and SCLoss is adopted together with FP16 training, numerical instability is frequently observed, regardless of whether gradient clipping is applied. After disabling SCLOSS, although the overall performance drops significantly, such instability is no longer observed. When we replace the loss function with our proposed SSCLoss ($\tau = 0.5$), the issue is mitigated significantly with gradient clipping. However, when gradient clipping is disabled, numerical instability re-emerges. This observation indicates that although the proposed SSCLoss is effective in mitigating gradient instability, it is insufficient on its own to fully stabilize gradient fluctuations under a high learning rate. Additionally, when FP32 training is adopted, numerical instability is rarely observed, which is consistent with our hypothesis that small gradients below the margin are more likely to underflow under mixed-precision training.

TABLE IV

ABLATION STUDY OF NUMERICAL INSTABILITY ON LANDSATSCD DATASET. GC DENOTES GRADIENT CLIPPING AND NI DENOTES NUMERICAL INSTABILITY.

Method	GC	Precision	Loss	F_{scd}	NI
PerASCD	1.5	FP16	-	80.39	No
PerASCD	1.5	FP16	L_{sc}	-	Yes
PerASCD	-	FP16	L_{sc}	-	Yes
PerASCD	-	FP32	L_{sc}	90.48	No
PerASCD	1.5	FP16	L_{ssc}	90.90	No
PerASCD	-	FP16	L_{ssc}	-	Yes
PerASCD	-	FP32	L_{ssc}	90.52	No

PerASCD - FP16 - 79.19 No

4) *Ablation Study of the Temperature Parameter τ* : We also conduct a bunch of ablation experiments to explore the effect of temperature parameter τ on both LandsatSCD and SECOND. The results indicate that the temperature parameter τ should be adjusted according to the distribution of the training dataset.

As shown in the Table V, since the LandsatSCD dataset exhibits a simpler data distribution with less noise, the model is less prone to overfitting. As a result, the best performance is achieved at a relatively high temperature value ($\tau = 0.5$), as weaker constraints allow the model to more effectively capture fine-grained details in a low-noise data regime. When temperature value τ achieved 0.01, the numerical instability is observed due to a strong constraint with high upgrade step size.

TABLE V
ABLATION STUDY OF THE TEMPERATURE PARAMETER TAU ON LANDSATSCD DATASET

Method	τ	OA	F_{scd}	mIoU	Sek
PerASCD	0.01	96.48	89.85	89.60	62.31
PerASCD	0.05	96.67	90.39	90.06	63.73
PerASCD	0.1	96.79	90.72	90.38	64.69
PerASCD	0.5	96.84	90.90	90.54	65.21
PerASCD	1	96.75	90.60	90.26	64.33

On the SECOND dataset, as shown in the Table VI, due to the complexity of SECOND dataset, a high temperature involved more noise information, leading to a limited performance. As the temperature τ is gradually decreased, the optimal F_{scd} performance consistently improves and reaches its peak at $\tau = 0.01$ or $\tau = 0.02$. Since a relatively smaller initial learning rate of 0.1 is adopted during training, the strong regularization imposed by SSCLoss, although closely resembling the original SCLOSS, does not lead to frequent numerical instability. In contrast, benefiting from improved regularization and smoother gradients, overfitting is substantially reduced, leading to a significant improvement in overall performance.

TABLE VI
ABLATION STUDY OF THE TEMPERATURE PARAMETER TAU ON SECOND DATASET, BOLD INDICATES THE BEST RESULT.

Method	τ	OA	F_{scd}	mIoU	Sek
PerASCD	0.005	88.30	66.33	74.30	26.17
PerASCD	0.01	88.70	66.41	74.33	26.11
PerASCD	0.02	88.65	66.45	74.45	26.23
PerASCD	0.1	88.34	66.36	74.32	26.21
PerASCD	0.5	88.53	66.33	74.33	26.10
PerASCD	1	88.36	66.32	74.28	26.12

V. DISCUSSION AND CONCLUSION

We proposed a novel SCD method leveraging PerA pre-trained foundation model and a simplified modular CG-decoder. Our method achieved state-of-the-art on two benchmark datasets, demonstrating the effectiveness of our approach. In addition, we conducted a bunch of ablation

> REPLACE THIS LINE WITH YOUR MANUSCRIPT ID NUMBER (DOUBLE-CLICK HERE TO EDIT) <

studies to explore the numerical instability in SCD, and investigate the feasibility of multiple RS foundation models for the SCD Tasks.

There remain several open questions worthy of further investigation. First, how to effectively adapt more complex multimodal pre-trained models to the SCD task remains an open challenge. Second, although the proposed CG-Decoder simplifies the SCD paradigm, it still requires explicit modeling and prediction of change features; whether this structure can be further simplified deserves further exploration. Third, while SSCLoss performs as expected, it introduces an additional hyperparameter τ that requires tuning, and how to optimize or eliminate this dependency remains an open question.

REFERENCES

- [1] S. Tian, A. Ma, Z. Zheng, and Y. Zhong, “Hi-UCD: A Large-scale Dataset for Urban Semantic Change Detection in Remote Sensing Imagery,” Dec. 28, 2020, *arXiv*: arXiv:2011.03247. doi: 10.48550/arXiv.2011.03247.
- [2] A. Ochytra, A. Marcinkowska-Ochytra, and E. Raczko, “Threshold- and trend-based vegetation change monitoring algorithm based on the inter-annual multi-temporal normalized difference moisture index series: A case study of the Tatra Mountains,” *Remote Sensing of Environment*, vol. 249, p. 112026, Nov. 2020, doi: 10.1016/j.rse.2020.112026.
- [3] Z. Zheng, Y. Zhong, J. Wang, A. Ma, and L. Zhang, “Building damage assessment for rapid disaster response with a deep object-based semantic change detection framework: From natural disasters to man-made disasters,” *Remote Sensing of Environment*, vol. 265, p. 112636, Nov. 2021, doi: 10.1016/j.rse.2021.112636.
- [4] K. Cha, J. Seo, and T. Lee, “A Billion-scale Foundation Model for Remote Sensing Images,” *IEEE J. Sel. Top. Appl. Earth Observations Remote Sensing*, pp. 1–17, 2024, doi: 10.1109/JSTARS.2024.3401772.
- [5] X. Sun *et al.*, “RingMo: A Remote Sensing Foundation Model With Masked Image Modeling,” *IEEE Trans. Geosci. Remote Sensing*, vol. 61, pp. 1–22, 2023, doi: 10.1109/TGRS.2022.3194732.
- [6] U. Mall, B. Hariharan, and K. Bala, “Change-Aware Sampling and Contrastive Learning for Satellite Images,” in *2023 IEEE/CVF Conference on Computer Vision and Pattern Recognition (CVPR)*, Vancouver, BC, Canada: IEEE, Jun. 2023, pp. 5261–5270. doi: 10.1109/CVPR52729.2023.00509.
- [7] H. Shen, H. Gu, H. Li, Y. Yang, and A. Qiu, “A Contrastive Learning Foundation Model Based on Perfectly Aligned Sample Pairs for Remote Sensing Images,” Jun. 24, 2025, *arXiv*: arXiv:2505.19447. doi: 10.48550/arXiv.2505.19447.
- [8] C. J. Reed *et al.*, “Scale-MAE: A Scale-Aware Masked Autoencoder for Multiscale Geospatial Representation Learning,” Sep. 22, 2023, *arXiv*: arXiv:2212.14532. doi: 10.48550/arXiv.2212.14532.
- [9] O. Mañas, A. Lacoste, X. Giro-i-Nieto, D. Vazquez, and P. Rodriguez, “Seasonal Contrast: Unsupervised Pre-Training from Uncurated Remote Sensing Data,” May 03, 2021, *arXiv*: arXiv:2103.16607. doi: 10.48550/arXiv.2103.16607.
- [10] X. Guo *et al.*, “SkySense: A Multi-Modal Remote Sensing Foundation Model Towards Universal Interpretation for Earth Observation Imagery,” Mar. 22, 2024, *arXiv*: arXiv:2312.10115. doi: 10.48550/arXiv.2312.10115.
- [11] R. Caye Daudt, B. Le Saux, and A. Boulch, “Fully Convolutional Siamese Networks for Change Detection,” in *2018 25th IEEE International Conference on Image Processing (ICIP)*, Oct. 2018, pp. 4063–4067. doi: 10.1109/ICIP.2018.8451652.
- [12] S. Fang, K. Li, J. Shao, and Z. Li, “SNUNet-CD: A Densely Connected Siamese Network for Change Detection of VHR Images,” *IEEE Geoscience and Remote Sensing Letters*, vol. 19, pp. 1–5, 2022, doi: 10.1109/LGRS.2021.3056416.
- [13] A. Dosovitskiy *et al.*, “An Image is Worth 16x16 Words: Transformers for Image Recognition at Scale,” Jun. 03, 2021, *arXiv*: arXiv:2010.11929. doi: 10.48550/arXiv.2010.11929.
- [14] H. Chen, Z. Qi, and Z. Shi, “Remote Sensing Image Change Detection With Transformers,” *IEEE Transactions on Geoscience and Remote Sensing*, vol. 60, pp. 1–14, 2022, doi: 10.1109/TGRS.2021.3095166.
- [15] W. G. C. Bandara and V. M. Patel, “A Transformer-Based Siamese Network for Change Detection,” in *IGARSS 2022 - 2022 IEEE International Geoscience and Remote Sensing Symposium*, Jul. 2022, pp. 207–210. doi: 10.1109/IGARSS46834.2022.9883686.
- [16] C. Wu, L. Zhang, and B. Du, “Kernel Slow Feature Analysis for Scene Change Detection,” *IEEE Trans. Geosci. Remote Sensing*, vol. 55, no. 4, pp. 2367–2384, Apr. 2017, doi: 10.1109/TGRS.2016.2642125.
- [17] T. Suzuki, S. Shirakabe, Y. Miyashita, A. Nakamura, Y. Satoh, and H. Kataoka, “Semantic Change Detection with Hypermaps,” Mar. 16, 2017, *arXiv*: arXiv:1604.07513. doi: 10.48550/arXiv.1604.07513.
- [18] A. Varghese, J. Gubbi, A. Ramaswamy, and P. Balamuralidhar, “ChangeNet: A Deep Learning Architecture for Visual Change Detection,” presented at the Proceedings of the European Conference on Computer Vision (ECCV) Workshops, 2018, pp. 0–0. Accessed: Feb. 05, 2026. [Online]. Available: https://openaccess.thecvf.com/content_eccv_2018_workshops/w7/html/Varghese_ChangeNet_A_Deep_Learning_Architecture_for_Visual_Change_Detection_ECCVW_2018_paper.html
- [19] R. Caye Daudt, B. Le Saux, A. Boulch, and Y. Gousseau, “Multitask learning for large-scale semantic change detection,” *Computer Vision and Image Understanding*, vol. 187, p. 102783, Oct. 2019, doi: 10.1016/j.cviu.2019.07.003.
- [20] Y. Wang, B. Du, L. Ru, C. Wu, and H. Luo, “Scene Change Detection VIA Deep Convolution Canonical Correlation Analysis Neural Network,” in *IGARSS 2019 - 2019 IEEE International Geoscience and Remote Sensing Symposium*, Yokohama, Japan: IEEE, Jul. 2019, pp. 198–201. doi: 10.1109/IGARSS.2019.8898211.
- [21] D. Peng, L. Bruzzone, Y. Zhang, H. Guan, and P. He, “SCDNET: A novel convolutional network for semantic change detection in high resolution optical remote sensing imagery,” *International Journal of Applied Earth Observation and Geoinformation*, vol. 103, p. 102465, Dec. 2021, doi: 10.1016/j.jag.2021.102465.
- [22] Y. Zhu, L. Li, K. Chen, C. Liu, F. Zhou, and Z. Shi, “Semantic-CD: Remote Sensing Image Semantic Change Detection towards Open-vocabulary Setting,” Jan. 12, 2025, *arXiv*: arXiv:2501.06808. doi: 10.48550/arXiv.2501.06808.
- [23] Y. Deng *et al.*, “Feature-Guided Multitask Change Detection Network,” *IEEE J. Sel. Top. Appl. Earth Observations Remote Sensing*, vol. 15, pp. 9667–9679, 2022, doi: 10.1109/JSTARS.2022.3215773.
- [24] S. Xiang, M. Wang, X. Jiang, G. Xie, Z. Zhang, and P. Tang, “Dual-Task Semantic Change Detection for Remote Sensing Images Using the Generative Change Field Module,” *Remote Sensing*, vol. 13, no. 16, p. 3336, Aug. 2021, doi: 10.3390/rs13163336.
- [25] L. Ding, J. Zhang, H. Guo, K. Zhang, B. Liu, and L. Bruzzone, “Joint Spatio-Temporal Modeling for Semantic Change Detection in Remote Sensing Images,” *IEEE Trans. Geosci. Remote Sensing*, vol. 62, pp. 1–14, 2024, doi: 10.1109/TGRS.2024.3362795.
- [26] L. Ding, H. Guo, S. Liu, L. Mou, J. Zhang, and L. Bruzzone, “Bi-Temporal Semantic Reasoning for the Semantic Change Detection in HR Remote Sensing Images,” *IEEE Trans. Geosci. Remote Sensing*, vol. 60, pp. 1–14, 2022, doi: 10.1109/TGRS.2022.3154390.
- [27] J. Wang *et al.*, “MSCD-Net: From Unimodal to Multimodal Semantic Change Detection,” *IEEE Trans. Geosci. Remote Sensing*, vol. 63, pp. 1–17, 2025, doi: 10.1109/TGRS.2025.3591814.
- [28] Q. Shu *et al.*, “Semantic Change Detection of Roads and Bridges: A Fine-grained Dataset and Multimodal Frequency-driven Detector,” Sep. 19, 2025, *arXiv*: arXiv:2505.13212. doi: 10.48550/arXiv.2505.13212.
- [29] B. Wijenayake *et al.*, “Mamba-FCS: Joint Spatio- Frequency Feature Fusion, Change-Guided Attention, and SEK Loss for Enhanced Semantic Change Detection in Remote Sensing,” Aug. 11, 2025, *arXiv*: arXiv:2508.08232. doi: 10.48550/arXiv.2508.08232.
- [30] X. Liu *et al.*, “GSTM-SCD: Graph-enhanced spatio-temporal state space model for semantic change detection in multi-temporal remote sensing images,” *ISPRS Journal of Photogrammetry and Remote Sensing*, vol. 230, pp. 73–91, Dec. 2025, doi: 10.1016/j.isprsjprs.2025.09.003.
- [31] Z. Chen *et al.*, “Vision Transformer Adapter for Dense Predictions,” Feb. 13, 2023, *arXiv*: arXiv:2205.08534. doi: 10.48550/arXiv.2205.08534.
- [32] O. Ronneberger, P. Fischer, and T. Brox, “U-Net: Convolutional Networks for Biomedical Image Segmentation,” in *Medical Image Computing and Computer-Assisted Intervention – MICCAI 2015*, N. Navab, J. Hornegger, W. M. Wells, and A. F. Frangi, Eds., Cham: Springer International Publishing, 2015, pp. 234–241. doi: 10.1007/978-3-319-24574-4_28.

> REPLACE THIS LINE WITH YOUR MANUSCRIPT ID NUMBER (DOUBLE-CLICK HERE TO EDIT) <

[33]K. Yang *et al.*, “Asymmetric Siamese Networks for Semantic Change Detection in Aerial Images,” *IEEE Trans. Geosci. Remote Sensing*, vol. 60, pp. 1–18, 2022, doi: 10.1109/TGRS.2021.3113912.

[34]P. Yuan, Q. Zhao, X. Zhao, X. Wang, X. Long, and Y. Zheng, “A transformer-based Siamese network and an open optical dataset for semantic change detection of remote sensing images,” *International Journal of Digital Earth*, vol. 15, no. 1, pp. 1506–1525, Dec. 2022, doi: 10.1080/17538947.2022.2111470.

[35]K. He, X. Zhang, S. Ren, and J. Sun, “Deep Residual Learning for Image Recognition,” presented at the Proceedings of the IEEE Conference on Computer Vision and Pattern Recognition, 2016, pp. 770–778. Accessed: Feb. 05, 2026. [Online]. Available: https://openaccess.thecvf.com/content_cvpr_2016/html/He_Deep_Residual_Learning_CVPR_2016_paper.html

[36]Z. Liu *et al.*, “Swin Transformer: Hierarchical Vision Transformer Using Shifted Windows,” presented at the Proceedings of the IEEE/CVF International Conference on Computer Vision, 2021, pp. 10012–10022. Accessed: Feb. 05, 2026. [Online]. Available: https://openaccess.thecvf.com/content/ICCV2021/html/Liu_Swin_Transformer_Hierarchical_Vision_Transformer_Using_Shifted_Windows_ICCV_2021_paper

[37]Y. Liu *et al.*, “VMamba: Visual State Space Model,” *Advances in Neural Information Processing Systems*, vol. 37, pp. 103031–103063, Dec. 2024, doi: 10.5220/079017-3273.

[38]Y. Cong *et al.*, “SatMAE: Pre-training Transformers for Temporal and Multi-Spectral Satellite Imagery”.



Hengtong Shen received the M.E. degree in photogrammetry and remote sensing from the Chinese Academy of Surveying and Mapping in 2025. He is currently pursuing a Ph.D. degree at Wuhan University.

His research interests include intelligent remote sensing interpretation, self-supervised learning for remote sensing, and deep learning.



Li Yan received the B.S., M.S., and Ph.D. degrees in photogrammetry and remote sensing from Wuhan University, Wuhan, China, in 1989, 1992, and 1999, respectively.

He is currently a Luojia Distinguished Professor with the School of Geodesy and Geomatics, Wuhan University. His research interests include 3-D reconstruction and measurement, real-time mobile mapping and surveying, intelligent remote sensing, and precise image measurement.



Hong Xie received the B.S., M.S., and Ph.D. degrees in photogrammetry and remote sensing from Wuhan University, Wuhan, China, in 2007, 2009, and 2013, respectively. He is currently an Associate Professor with the School of Geodesy and Geomatics, Wuhan University.

His research interests include target detection based on image deep learning, point cloud data quality improvement, point cloud information extraction and model reconstruction, mobile mapping, and surveying.



Yaxuan Wei received the M.E. degree in Surveying and Mapping from Beijing University of Civil Engineering and Architecture in 2025.

Her research interests include 3D change detection, semantic segmentation, and deep learning.



Xinhao Li received the M.E. degree in Surveying and Mapping from China University of Petroleum (East China) in 2025.

His research interests include 3D semantic segmentation, intelligent remote sensing interpretation, and deep learning.



Wenfei Shen received the M.E. degree in Surveying and Mapping from Beijing University of Civil Engineering and Architecture in 2025.

His research interests include 3D gaussian splatting reconstruction, temporal reconstruction, and deep learning.



Peixian Lv received the B.E. degree in surveying and mapping engineering from Nanjing Normal University in 2025. She is currently pursuing a M.E. degree at Wuhan University.

Her research interests focus on 3D change detection.



Fei Tan received his B.E. degree in remote sensing science and technology from Southwest Jiaotong University in 2024. He is currently pursuing a M.E. degree at Wuhan University.

His research interests include change detection in urban scenes and point cloud deep learning.